Ballistic near-field heat transport in dense many-body systems

Ivan Latella, Svend-Age Biehs, Riccardo Messina, Alejandro W. Rodriguez, and Philippe Ben-Abdallah

Ballistic near-field heat transport in dense many-body systems

Ivan Latella,[1] Svend-Age Biehs,[2] Riccardo Messina,[3, 4] Alejandro W. Rodriguez,[4] and Philippe Ben-Abdallah[1, 5, *]

[1]*Laboratoire Charles Fabry, UMR 8501, Institut d'Optique, CNRS,*
Université Paris-Saclay, 2 Avenue Augustin Fresnel, 91127 Palaiseau Cedex, France
[2]*Institut für Physik, Carl von Ossietzky Universität, D-26111 Oldenburg, Germany*
[3]*Laboratoire Charles Coulomb (L2C), UMR 5221 CNRS-Université de Montpellier, F- 34095 Montpellier, France*
[4]*Department of Electrical Engineering, Princeton University, Princeton, NJ 08544, USA*
[5]*Université de Sherbrooke, Department of Mechanical Engineering, Sherbrooke, PQ J1K 2R1, Canada.*

Radiative heat-transport mediated by near-field interactions is known to be superdiffusive in dilute, many-body systems. Here we use a generalized Landauer theory of radiative heat transfer in many-body planar systems to demonstrate a nonmonotonic transition from superdiffusive to ballistic transport in dense systems. We show that such a transition is associated to a change of the polarization of dominant modes. Our findings are complemented by a quantitative study of the relaxation dynamics of the system in the different regimes of heat transport. This result could have important consequences on thermal management at nanoscale of many-body systems.

I. INTRODUCTION

The theory of near-field radiative heat transfer has for many decades remained largely limited to two-body systems [1–6]. Recently, heat transport in many-body systems has also been considered in the context of nanoparticles [7–10] and multilayer geometries, such as photonic crystals [11, 12] and hyperbolic metamaterials [13–15]. The focus of much of this work has been the study of systems in which the steady-state temperature distribution of a set of internal bodies is a priori known and dictated via contact with large heat reservoirs. There are, however, situations in which a full study of heat transport necessitates an account of thermal relaxation through radiative channels. A first step in this direction has been made by generalizing Rytov's theory of fluctutational electrodynamics to describe radiative transfer in many-body geometries with varying temperature distributions, including nanoparticle systems [17–19], multilayer configurations [16, 20–28], and more generally, arbitrary geometries that include the possibility of inhomogeneously varying temperature profiles [29, 30]. Furthermore, so far, only a superdiffusive regime of heat transport has been observed in systems purely driven by thermal radiation and, in particular, only in nanoparticle systems within the dipolar approximation [31].

In the present work, we employ a recently developed, exact theoretical framework [32] to investigate near-field radiative heat transport in N-body systems consisting of parallel planar slabs separated by vacuum, in which radiation is the only source of thermal relaxation. Here we restrict our discussion to polar materials, where the screening is weak enough to permit a long-range coupling between the constituent parts of the system. We show that the temperature dynamics and steady-state profile of the system depend strongly on geometric parameters such as the system density, which imply dif-

ferent heat-transport regimes. In particular, we prove the existence of a nonmonotonic transition between a superdiffusive regime, previously observed in Ref. [31], and a ballistic regime that appears in denser media and that also leads to dramatically faster relaxation dynamics. We also show that this transition is associated with a change in the polarization of the dominant modes in the transport. In contrast to heat exchange in two-body geometries, where near-field heat transfer is dominated by transverse-magnetic (TM) modes, we found that transport in dense, many-body systems can have a significant contribution from transverse-electric (TE) modes.

The rest of the paper is organized as follows. In Sec. II, we introduce the system under consideration and discuss a procedure to characterize the regime of heat transport. In Sec. III, we study the relaxation dynamics of the system for different configurations. For comparison purposes, in Sec. IV, we evaluate the large-distance behavior of the heat-transfer coefficients in a metal. Finally, our conclusions are summarized in Sec. V.

II. HEAT TRANSPORT REGIMES

Let us consider a system composed of N planar slabs separated by vacuum, orthogonal to the z axis and assumed to be infinite in the x and y directions, as sketched in Fig. 1(a). The thicknesses δ_j of the bodies are assumed to be equal, $\delta_j = \delta$ for $j = 1, \ldots, N$, and below we take $\delta = 200\,\text{nm}$. The temperatures of slabs 1 and N, referred to as *external* slabs, are held constant at $T_1 = 400\,\text{K}$ and $T_N = 300\,\text{K}$, respectively, via contact with an external reservoir, while all the other *internal* slabs are allowed to reach their own equilibrium temperature T_j^{eq} ($j = 2, ..., N - 1$). We also consider that the system is immersed in an environment (thermal bath) at temperature $T_0 = T_{N+1} = T_B = 300\,\text{K}$. Below D denotes the distance between slabs 1 and 2, as well as slabs $N - 1$ and N, whereas d is the distance between adjacent, internal slabs. Furthermore, in our numerical

simulations we assume that all the bodies are made of silicon carbide (SiC), whose permittivity at frequency ω can be described by the Drude-Lorentz model [33]

$$\varepsilon(\omega) = \varepsilon_\infty \frac{\omega_L^2 - \omega^2 - i\Gamma\omega}{\omega_T^2 - \omega^2 - i\Gamma\omega}, \qquad (1)$$

where $\varepsilon_\infty = 6.7$ is the high frequency dielectric constant, $\omega_L = 1.83 \times 10^{14}\,\mathrm{rad/s}$ is the longitudinal optical phonon frequency, $\omega_T = 1.49 \times 10^{14}\,\mathrm{rad/s}$ is the transverse optical phonon frequency, and $\Gamma = 8.97 \times 10^{11}\,\mathrm{rad/s}$ is the damping rate (for comparison purposes, in Sec. IV we also consider gold slabs). As shown in Ref. [32], the net radiative flux per unit surface received by any given slab j can be written as a sum over the energy exchanged with every other body $\varphi_{\ell,j}$, with

$$\varphi_j = \sum_{\ell \neq j} \varphi_{\ell,j} = \sum_{\ell \neq j} \int_0^\infty \frac{d\omega}{2\pi} \int_0^\infty \frac{dk}{2\pi} k \sum_p \hbar\omega\, n_{\ell,j} \mathcal{T}^{\ell,j}, \quad (2)$$

where $\ell \neq j$ runs from 0 to $N+1$ (including the external environment). In this expression $p = \mathrm{TE}, \mathrm{TM}$ denotes the two polarizations, k is the parallel component of the wave vector, and $n_{\ell,j} \equiv n_\ell - n_j$, with $n_j = \left(e^{\hbar\omega/k_B T_j} - 1\right)^{-1}$ denoting the Bose distribution. The Landauer coefficient $\mathcal{T}^{\ell,j} = \mathcal{T}^{\ell,j}(\omega, k, p)$, which can vary between 0 and 1, describes the contribution of each mode (ω, k, p) to the energy exchange and depends on the geometrical and material properties of the slabs [32]. The local equilibrium temperatures T_j^{eq} of the internal slabs can be calculated by requiring that in the steady state, the net flux received by each slab is zero, that is by solving the system of transcendental equations, $\varphi_j = 0$ for $j = 2, \ldots, N-1$. The steady-state temperature profiles inside the system are shown in Fig. 1(b) for $N = 60$ slabs and for several separation distances $d \in \{5, 40, 500\}\,\mathrm{nm}$ and fixed $D = 500\,\mathrm{nm}$. We first observe that, while for $d = D = 500\,\mathrm{nm}$ the temperature profile decays smoothly, the configurations having a smaller d reveal a more dramatic jump between the external and the adjacent (T_2, T_{N-1}) temperatures, in which case the internal slabs become much more thermally isolated from the reservoirs. Moreover, the shape of the profile clearly depends on d, becoming nonlinear for $d = 500\,\mathrm{nm}$, close to linear for $d = 40\,\mathrm{nm}$, and nearly constant for $d = 5\,\mathrm{nm}$.

We now describe how the main features characterizing heat transport in this geometry, i.e. the temperature profile near the boundary and within the bulk, depend on both D and d. As far as the former is concerned, the main parameter of interest is the relative coupling strength of boundary versus internal slabs, quantified by defining an effective, thermal conductivity

$$\kappa_j = \frac{\varphi_{j,j+1} d_j}{(T_j - T_{j+1})}, \qquad (3)$$

where $d_1 = d_{N-1} = D$ and $d_j = d$ for $j = 2, \ldots, N-2$. The ratio κ_j/κ_1, which can be interpreted as a measure of
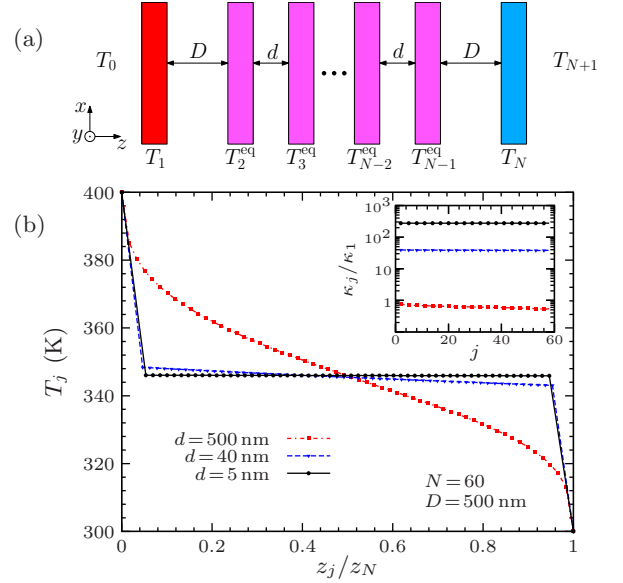

FIG. 1. (a) Schematic of an N-body system comprising $N-2$ planar slabs (purple) interacting with one another and with two external slabs at fixed temperatures T_1 (red) and T_N (blue). All internal separation distances d are identical while the coupling to the external thermostats depends on the separation distance D. In the steady state, each internal slab reaches a local equilibrium temperature T_j^{eq}. (b) Steady-state temperature profile as a function of the normalized position z_j/z_N for a system of $N = 60$ SiC slabs of thickness $200\,\mathrm{nm}$, for different d and fixed $D = 500\,\mathrm{nm}$. The inset shows the ratio of the effective internal conductivities κ_j/κ_1 (see text).

the boundary thermal resistance, is plotted in the inset of Fig. 1(b), showing that κ_j is almost constant within the chain of internal slabs and that κ_j/κ_1 is close to unity for $d = 500\,\mathrm{nm}$, increases with decreasing d, and reaches two orders of magnitude when $d = 5\,\mathrm{nm}$. As illustrated in Fig. 3 below, the smoothness of the temperature profile near the boundary only depends on the ratio d/D. We next focus on the shape of the temperature profile within the bulk, which is closely related to the transport regime and requires a more nuanced description of the problem.

As shown in Ref. [31], to understand and classify the various transport regimes in this kind of system, it is useful to study the power exchanged between layers in the limit of large N. For convenience, we make the simplifying assumption that the temperature differences involved in the system are small enough to allow a linearization of $n_{\ell,j}$. Under this assumption, the net flux on slab j reads,

$$\varphi_j \simeq \sum_{\ell \neq j} h_{\ell,j}(T_\ell - T_j), \qquad (4)$$

where we have introduced the heat-transfer coefficients,

$$h_{\ell,j} = \int_0^\infty \frac{d\omega}{2\pi} \int_0^\infty \frac{dk}{2\pi} k \sum_p \hbar\omega \frac{\partial n_j}{\partial T_j} \mathcal{T}^{\ell,j}. \qquad (5)$$

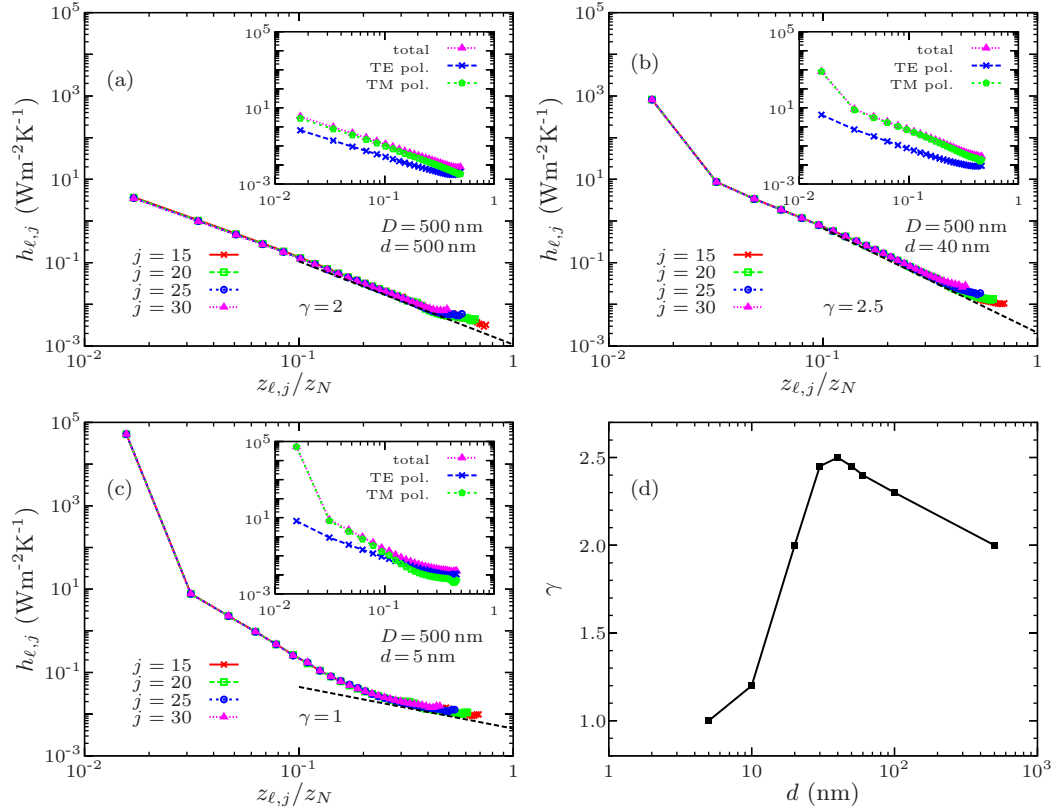Assuming that $h_{\ell,j} \sim 1/z_{\ell,j}^\gamma$, for some exponent $\gamma = 1+\alpha$,

FIG. 2. Heat-transfer coefficients $h_{\ell,j}$ (see text) with respect to the normalized separation $z_{\ell,j}/z_N$, for fixed values of j and $D = 500$ nm, and three values of (a) $d = 500$ nm, (b) $d = 40$ nm and (c) $d = 5$ nm. Dashed lines indicate the asymptotic behavior of $h_{\ell,j} \sim 1/z_{\ell,j}^\gamma$ at large separations. The value of γ indicates the nature of the heat-transport regime, from superdiffusive ($1 < \gamma < 3$) to ballistic ($\gamma \to 1$). The insets decompose $h_{\ell,j}$ for $j = 30$ into TE and TM polarization contributions. (d) Exponent γ as a function of d.

where $z_{\ell,j} \equiv |z_\ell - z_j|$ and z_j denotes the position of the j-th layer, one finds that in the thermodynamic limit $N \to \infty$, total length $L \to \infty$, and N/L fixed (see the Appendix for details), $T_j \to T(z)$ and

$$\varphi_j \to \varphi(z) \sim (-\Delta)^{\alpha/2} T(z), \qquad (6)$$

where $(-\Delta)^{\alpha/2}$ is the fractional Laplacian defined in 1D systems as ($0 < \alpha < 2$)

$$(-\Delta)^{\alpha/2} T(z) = c_\alpha \, \mathrm{PV} \int_{-\infty}^{\infty} \frac{T(z) - T(z')}{|z - z'|^{1+\alpha}} dz', \quad (7)$$

with c_α a constant [34, 35] and where PV denotes the principal value. As we discuss below, Eq. (7) can be used as a tool to relate the asymptotic, large-distance behavior of $h_{\ell,j}$ to the regime of heat transport. It follows from Eq. (7) that the regime of heat transport is superdiffusive when $1 < \gamma < 3$. In the limiting case $\gamma \to 3$, the fractional Laplacian degenerates into its classical form and the regime of transport is diffusive. On the other hand, as $\gamma \to 1$, the fractional Laplacian approaches the identity operator and the transport becomes ballistic.

Figure 2 shows $h_{\ell,j}$ for multiple values of j as a function of ℓ, for the same system of Fig. 1. When $d = 500$ nm,

corresponding to a SiC volume fraction of 28.5% (dilute system), $h_{\ell,j}$ asymptotically decays as $1/z_{\ell,j}^2$, showing that indeed the heat transport is superdiffusive, as in simple dipolar systems [31]. Note that the small variations in $h_{\ell,j}$ at the extreme end of the curves come from finite-size effects and are therefore not taken into account in the scaling analysis. When $d = 40$ nm [see Fig. 2(b)], the exponent in the scaling of $h_{\ell,j}$ increases, but the transport regime remains superdiffusive. On the other hand, when $d = 5$ nm, corresponding to a SiC volume fraction of 97.5% (dense system), $h_{\ell,j} \sim 1/z_{\ell,j}$, in which case the transport is ballistic and the system experiences an effectively weak thermal resistance within the bulk. Figure 2(d) shows γ as a function of d, illustrating a nonmonotonic behavior as the system transitions from a superdiffusive to a ballistic regime. Furthermore, as illustrated on the insets of Fig. 2, which show the contributions of TE and TM modes to $h_{\ell,j}$, we find that TE modes dominate and hence determine the (ballistic) transport regime at small d; in contrast, TM modes are the main heat carriers in the superdiffusive regime, which is the case in typical two-body geometries involving polaritonic resonances. This surprising result is a clear indication of the complexities and richness of heat trans-
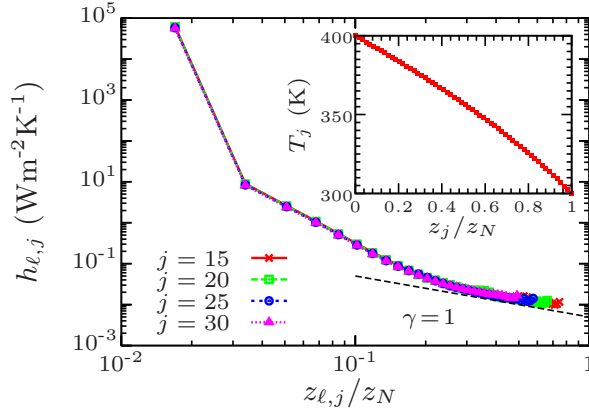
FIG. 3. Heat-transfer coefficients $h_{\ell,j}$ as a function of the normalized separation $z_{\ell,j}/z_N$, for $D = d = 5$ nm, along with the corresponding steady-state temperature profile (inset).
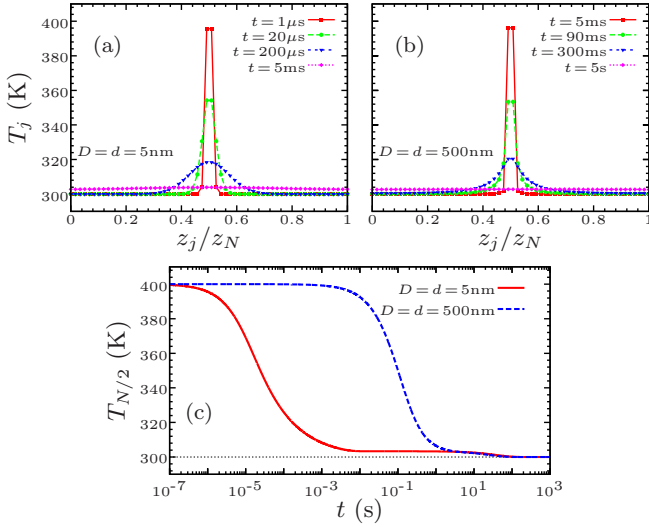

FIG. 4. Temporal evolution of the temperature profile for a system ($N = 60$) interacting with a thermal bath at $T_B = T_0 = T_{N+1} = 300$ K. At $t = 0$, all bodies have temperature T_B except the two central slabs, which have $T_{N/2} = T_{N/2+1} = 400$ K. (a) Ballistic regime ($D = d = 5$ nm). (b) Superdiffusive regime ($D = d = 500$ nm). (c) Temperature of slab $N/2$ as a function of time in the two previous cases.

port in many-body systems. We remark that for metals at room temperature (far from the plasmon resonance), the screening is so strong that interactions in the structure can be effectively short-ranged. As a consequence of the screening, the heat-transfer coefficients may exhibit an exponential decay rather than a power-law decay (see Sec. IV), and therefore our model for anomalous diffusion does not apply in this case.

Figure 3 shows $h_{\ell,j}$ along with the temperature profile (inset) for $d = D = 5$ nm. Comparing the former to the results in Fig. 2(c), one confirms that the transport regime is independent of D and therefore only depends on the density within the bulk, determined by d. On the

other hand, comparing the temperature profile in Fig. 3 to those in Fig. 1, one infers that indeed only the ratio d/D (or thermal resistance) controls the smoothness of the profile near the boundaries.

III. THERMAL RELAXATION

We now investigate the impact of the previously considered transport regimes on the relaxation dynamics of the system. Given an initial temperature distribution $\boldsymbol{T}(0) = \big(T_1(0), ..., T_N(0)\big)$, the temperatures of the bodies $\boldsymbol{T}(t) = \big(T_1(t), \ldots, T_N(t)\big)$ at any give time $t > 0$ are solutions of the energy balance equation,

$$\partial_t \boldsymbol{T} = \mathbb{K} \cdot \boldsymbol{T} + \boldsymbol{S}, \tag{8}$$

where $\mathbb{K} = \mathbb{H}/(C\delta)$ is a stiffness matrix defined in terms of the heat-transfer matrix $\mathbb{H}$, with elements $[\mathbb{H}]_{\ell,j} = h_{\ell,j}$ ($\ell, j = 1, \ldots, N$), and $C = 8.15$ J·cm^{-3}·K^{-1} is the SiC heat capacity per unit volume [36]. Here, $h_{j,j} = -\sum_{\ell \neq j} h_{\ell,j}$ quantifies the emission rate of body j in the presence of the other slabs, while $\boldsymbol{S} = \frac{T_B}{C\delta}(h_{0,1} + h_{N+1,1}, \ldots, h_{0,N} + h_{N+1,N})$ denotes the source term corresponding to power supplied by the baths to each layer. Equation (8) is simply a discrete form of the fractional diffusion equation, the fractional exponent being related to the scaling of $h_{\ell,j}$, whose solution in the steady state reads

$$\boldsymbol{T}^{\text{eq}} = -\mathbb{K}^{-1} \cdot \boldsymbol{S} = (T_B, \ldots, T_B). \tag{9}$$

Since $h_{\ell,j}$ depends weakly on T_j, we assume that $\mathbb{K}$ is a time-independent matrix, in which case the time evolution of the temperature profile is given by

$$\boldsymbol{T}(t) = \exp(\mathbb{K}t) \cdot [\boldsymbol{T}(0) - \boldsymbol{T}^{\text{eq}}] + \boldsymbol{T}^{\text{eq}}. \tag{10}$$

Figure 4 shows the temporal evolution of the system in both superdiffusive and ballistic regimes, assuming an initial temperature profile corresponding to heating of the two central slabs to a temperature of 400 K. We observe a strong increase of the relaxation dynamics in the ballistic regime compared to the superdiffusive case, showing a difference in characteristic equilibration scales of nearly three orders of magnitude (from microseconds to milliseconds for a reduction of about half the initial overheating). We also observe that, as previously observed in dilute media [17], the relaxation process occurs in two distinct timescales. First, all layers thermalize at the same temperature through near-field interactions in about 5 ms in dense media (seconds in the diluted case). Subsquently, all layers collectively cool down to the ambient temperature through far-field interactions with the thermal bath.
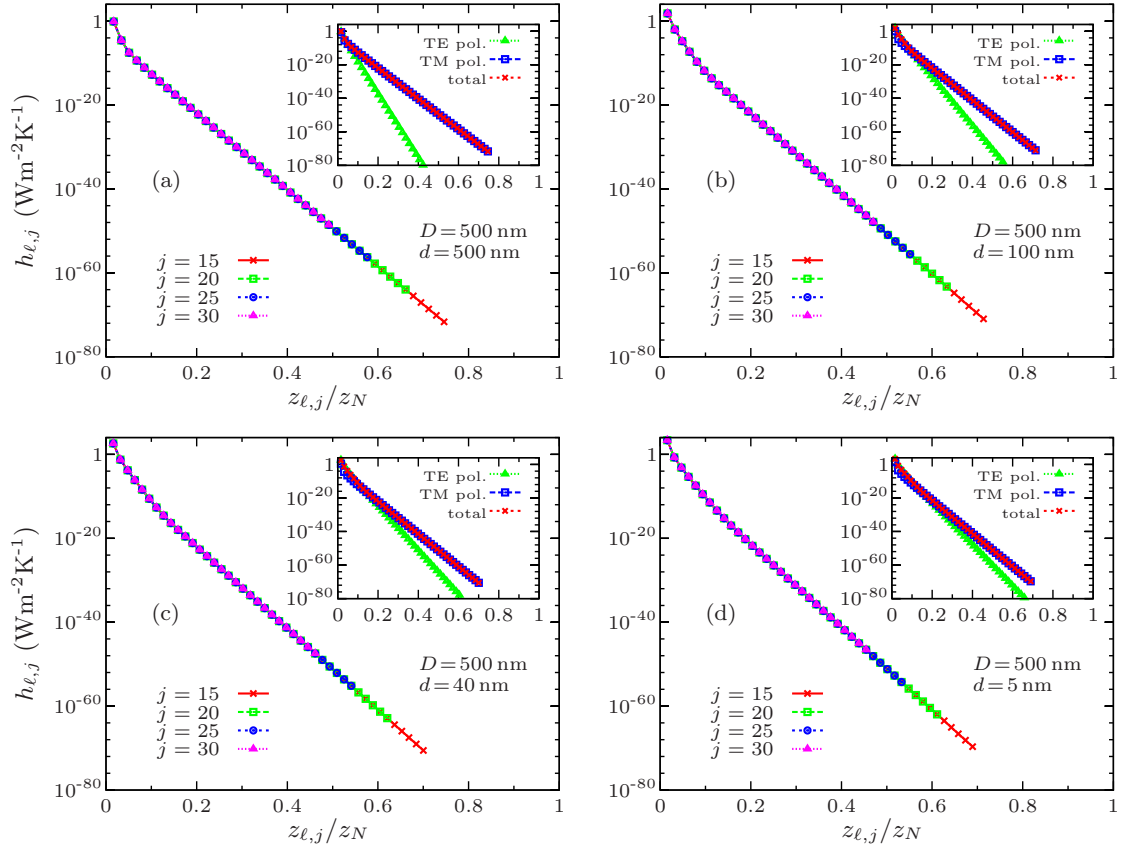
FIG. 5. Heat-transfer coefficients $h_{\ell,j}$ for gold slabs with respect to the normalized separation $z_{\ell,j}/z_N$ for fixed values of j. Here $D = 500\,\text{nm}$ and (a) $d = 500\,\text{nm}$, (b) $d = 100\,\text{nm}$, (c) $d = 40\,\text{nm}$, and (d) $d = 5\,\text{nm}$. At large $z_{\ell,j}$, an exponential decay is clearly observed. The insets decompose $h_{\ell,j}$ for $j = 15$ into TE and TM polarization contributions.

IV. HEAT-TRANSFER COEFFICIENTS FOR GOLD SLABS

In this section we analyze the heat-transfer coefficients for the same geometrical configurations discussed previously, but now taking gold (Au) as the material constituting the slabs. The permittivity of Au is described with a Drude model

$$\varepsilon(\omega) = 1 - \frac{\omega_P^2}{\omega(\omega + i\Gamma)}, \tag{11}$$

with plasma frequency $\omega_P = 1.37 \times 10^{16}\,\text{rad/s}$ and dissipation rate $\Gamma = 5.32 \times 10^{13}\,\text{rad/s}$. The width of the bodies is assumed $\delta = 200\,\text{nm}$, the separation distance between bodies 1 and 2 and between bodies $N - 1$ and N is taken as $D = 500\,\text{nm}$, with $N = 60$. In Fig. 5, we show the heat-transfer coefficients with respect to the normalized separation $z_{\ell,j}/z_N$ for fixed values of j and several values of the internal spacing d, where, as before, $z_{\ell,j} = |z_\ell - z_j|$. As shown in the plots, the heat-transfer coefficients for this metal exhibit an exponential decay at large separations, which contrasts with the power-law behavior observed in the polar material. The reason for that is the strong screening taking place in the metal. For

this material and under these conditions, our model for anomalous diffusion does not apply; in this case, the radiative heat transport is driven by effective, short-range interactions. We emphasize that the dependence of the decay on $z_{\ell,j}$ may be different for thinner slabs, since in this case the electromagnetic field is less attenuated.

d (nm)	α_0 (nm^{-1})	δ_0 (nm)
5	1.74×10^{-2}	115
40	1.48×10^{-2}	135
100	1.19×10^{-2}	169
500	5.08×10^{-3}	394

TABLE I. Calculated values of the absorption coefficient α_0 and skin depth δ_0 as a function of d for Au slabs.

According to our numerical results, assuming a continuous distribution of bodies, for the metal the heat transfer coefficients can be written as

$$h \sim e^{-\alpha_0 z}, \tag{12}$$

where α_0 can be interpreted as an absorption coefficient. Thus, we can define a skin depth [37]
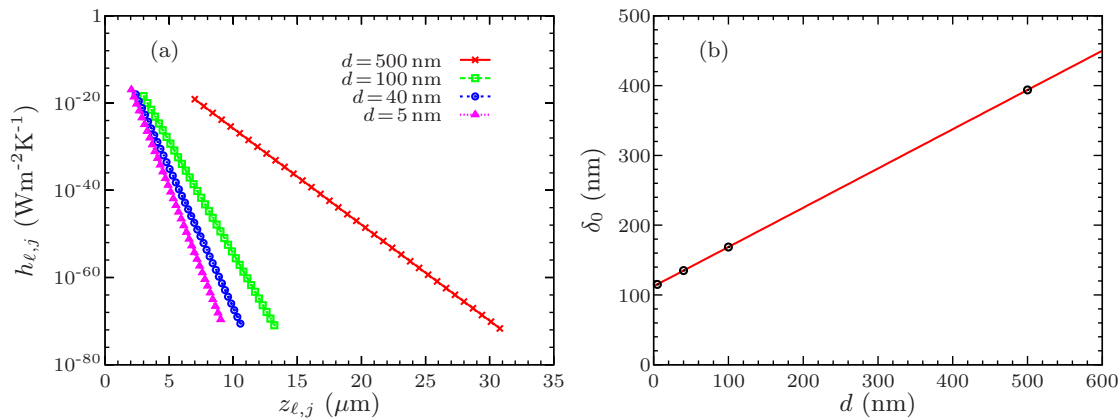
$$\delta_0 = \frac{2}{\alpha_0}, \tag{13}$$

FIG. 6. (a) Large-distance behavior of the heat-transfer coefficients $h_{\ell,j}$ for Au slabs with respect to the separation $z_{\ell,j} = |z_\ell - z_j|$ for $j = 15$ and several values of the spacing d. (b) Skin depth δ_0 as a function of d (see Table I). The limit $d \to 0$ can be extrapolated from a linear fitting, leading to $\delta_0 \approx 112\,\text{nm}$.

which for bulk metals at room temperature is typically about $100\,\text{nm}$. In Table I, we report the values of the absorption coefficient α_0 and the skin depth δ_0 for $d = 5\,\text{nm}$, $d = 40\,\text{nm}$, $d = 100\,\text{nm}$, and $d = 500\,\text{nm}$. The values of α_0 are obtained by fitting the large-distance behavior of the heat-transfer coefficients shown in Fig. 6(a). In Fig. 6(b), we show that d and δ_0 follow a linear relation. The expected value of δ_0 for the bulk can be obtained in the limit $d \to 0$, which can be extrapolated from a linear fitting [see Fig. 6(b)]. In this limit, we get $\delta_0 \approx 112\,\text{nm}$, which is consistent with the previously mentioned typical value.

V. CONCLUSIONS

We have studied a many-body geometry of planar slabs which exhibits a transition in the regime of radiative heat transport, from ballistic to superdiffusive, with respect to slab density. This transition has been found in a polar material, where the screening is weak and a long-range photon-mediated heat exchange takes place through the system. Because of the long-range coupling, the decay of the heat-transfer coefficients through the structure is characterized by a power law whose exponent determines the anomalous regime of heat transport. In many-body systems composed of metals, on the contrary, we have shown that the heat transfer coeffcients can decay exponentially and hence anomalous diffusion is not observed. In this case, the radiative transport is driven by short-range interactions. Furthermore, our predictions reveal complex, many-body effects in addition to dramatically different relaxation dynamics, depending on the transport regime. These effects could have important implications for thermal management at nanoscale in devices involving multiple, interacting elements thermally coupled in the near field.

Appendix: Thermodynamic limit

Here we perform the derivation of the energy balance equation (4) in the thermodynamic limit which leads to Eq. (6). We assume that the system is large enough so that we can take the total length $L \to \infty$ and the number of bodies $N \to \infty$, with the linear density $\lambda = N/L$ fixed. In doing so, the positions of the bodies can be continuously described by $z_j \to z$, and the flux, temperature, and heat-transfer coefficients become functions of the position such that $\varphi_j \to \varphi(z)$, $T_j \to T(z)$, and $h_{\ell,j} \to h(z,z')$, respectively. In addition, in the thermodynamic limit, the summation over the bodies in Eq. (4) can be expressed as

$$\lim_{N \to \infty} \sum_{\ell \neq j} \to \lim_{\substack{N \to \infty \\ L \to \infty}} \frac{N}{L} \, \text{PV} \int_{-L/2}^{L/2} dz' = \lambda \, \text{PV} \int_{-\infty}^{\infty} dz',$$

(A.1)

where PV denotes the principal value which needs to be used because the sum does not include $\ell = j$. Equation (4) then becomes

$$\varphi(z) = -\lambda \, \text{PV} \int_{-\infty}^{\infty} h(z,z') \left[T(z) - T(z') \right] dz'. \quad \text{(A.2)}$$

Identifying the heat-transfer coefficients in the thermodynamic limit from their discrete counterpart could be a difficult task. However, here we are only interested in the asymptotic, large distance behavior of these coefficients,

namely, when $|z - z'|$ is large. As an ansatz, we assume that $h(z, z') = q/|z - z'|^{1+\alpha}$, where q is some constant and $0 < \alpha < 2$. According to the numerical simulations shown in Sec. II, this assumption is well justified since the system exhibit anomalous diffusion. Therefore

$$\varphi(z) = -q\lambda \, \text{PV} \int_{-\infty}^{\infty} \frac{T(z) - T(z')}{|z - z'|^{1+\alpha}} dz'. \qquad (A.3)$$

Finally, introducing the fractional Laplacian $(-\Delta)^{\alpha/2}$ for 1-dimensional systems through the identity (7), the heat flux can be written as

$$\varphi(z) = -\frac{q\lambda}{c_\alpha}(-\Delta)^{\alpha/2}T(z), \qquad (A.4)$$

with the constant $c_\alpha = 2^\alpha \Gamma(\frac{\alpha+1}{2})/[\pi^{1/2}|\Gamma(-\frac{\alpha}{2})|]$, $\Gamma(x)$ being the Gamma function.

[1] D. Polder and M. van Hove, Phys. Rev. B **4**, 3303 (1971).
[2] J. J. Loomis and H. J. Maris, Phys. Rev. B **50**, 18517 (1994).
[3] K. Joulain, J.-P. Mulet, F. Marquier, R. Carminati, and J.-J. Greffet, Surf. Sci. Rep. **57**, 59 (2005).
[4] A. I. Volokitin and B. N. J. Persson, Rev. Mod. Phys. **79**, 1291 (2007).
[5] C. R. Otey, L. Zhu, S. Sandhu, and S. Fan, J. Quant. Spec. Rad. Trans. **132**, 3 (2014).
[6] B. Song, A. Fiorino, E. Meyhofer, and P. Reddy. AIP Advances **5**, 053503 (2015).
[7] P. Ben-Abdallah, Appl. Phys. Lett. **89**, 113117 (2006).
[8] P. Ben-Abdallah, K. Joulain, J. Drevillon and C. Le Goff, Phys. Rev. B **77**, 075417 (2008).
[9] P. Ben-Abdallah, S.-A. Biehs, and K. Joulain, Phys. Rev. Lett. **107**, 114301 (2011).
[10] J. Ordonez-Miranda, L. Tranchant, K.Joulain, Y. Ezzahri, J. Drevillon, and S. Volz, Phys. Rev. B **93**, 035428 (2016).
[11] W. T. Lau, J.-T. Shen, G. Veronis, S. Fan, and P. V. Braun, Appl. Phys. Lett. **92**, 103106 (2008).
[12] W. T. Lau, J.-T. Shen, and S. Fan, Phys. Rev. B **80**, 155135 (2009).
[13] J. Liu and E. Narimanov, Phys. Rev. B **91**, 041403(R) (2015).
[14] S.-A. Biehs, S. Lang, A. Yu. Petrov, M. Eich, and P. Ben-Abdallah, Phys. Rev. Lett. **115**, 174301 (2015).
[15] R. Messina, P. Ben-Abdallah, B. Guizal, M. Antezza and S.-A. Biehs, Phys. Rev. B **94**, 104301 (2016).
[16] R. Messina, M. Antezza, and P. Ben-Abdallah, Phys. Rev. Lett. **109**, 244302 (2012).
[17] R. Messina, M. Tschikin, S.-A. Biehs, and P. Ben-Abdallah, Phys. Rev. B **88**, 104307 (2013).
[18] V. Yannopapas and N. V. Vitanov, Phys. Rev. Lett. **110**, 044302 (2013).
[19] M. Nikbakht, EPL **110**, 14004 (2015).
[20] V. Kubytskyi, S.-A. Biehs, and P. Ben-Abdallah, Phys. Rev. Lett. **113**, 074301 (2014).
[21] R. Messina and M. Antezza, Phys. Rev. A **89**, 052104 (2014).
[22] P. Ben-Abdallah and S. A. Biehs, Phys. Rev. Lett. **112**, 044301 (2014)
[23] S. A. Dyakov, J. Dai, M. Yan, and M. Qiu, J. Phys. D: Appl. Phys. **48**, 305104 (2015)..
[24] I. Latella, A. Pérez-Madrid, J. M. Rubi, S.-A. Biehs, and P. Ben-Abdallah, Phys. Rev. Applied **4**, 011001 (2015).
[25] P. Ben-Abdallah, Phys. Rev. Lett. **116**, 084301 (2016).
[26] B. Müller, R. Incardone, M. Antezza, T. Emig, and M. Krüger, Phys. Rev. B **95**, 085413 (2017).
[27] R. Messina, W. Jin and A. W. Rodriguez, Phys. Rev. B **94**, 205438 (2016).
[28] R. Messina, W. Jin and A. W. Rodriguez, Phys. Rev. B **94**, 121410(R) (2016).
[29] S. Edalatpour and M. Francoeur, Phys. Rev. B **94**, 045406 (2016).
[30] W. Jin, R. Messina, and A. W. Rodriguez, Phys. Rev. B **95**, 161409(R) (2017).
[31] P. Ben-Abdallah, R. Messina, S.-A. Biehs, M. Tschikin, K. Joulain, and C. Henkel, Phys. Rev. Lett. **111**, 174301 (2013).
[32] I. Latella, P. Ben-Abdallah, S.-A. Biehs, M. Antezza and R. Messina, Phys. Rev. B **95**, 205404 (2017).
[33] *Handbook of Optical Constants of Solids*, edited by E. Palik (Academic Press, New York, 1998).
[34] I. Podlubny, *Fractional Differential Equations* (Academic Press, London, 1999).
[35] S. G. Samko, A. A. Kilbas, and O. I. Maritchev, *Fractional Integrals and Derivatives* (Gordon and Breach, New York, 1993).
[36] A. Sommers, Q. Wang, X. Han, C. T'Joen, Y. Park, and A. Jacobi, Appl. Therm. Eng. **30**, 1277 (2010).
[37] S. A. Maier, *Plasmonics: Fundamentals and Applications* (Springer, New York, 2007).